Temperature influence on layered double hydroxide tailored corncob biochar and its application for fluoride removal in aqueous media☆

Oshadi Hettithanthri [a,b], Anushka Upamali Rajapaksha [a,c], Nadeeshani Nanayakkara [d], Meththika Vithanage [a,e,f,*]

[a] Ecosphere Resilience Research Center, Faculty of Applied Sciences, University of Sri Jayewardenepura, Nugegoda 10250, Sri Lanka
[b] Postgraduate Institute of Sciences, University of Peradeniya, Peradeniya 20400, Sri Lanka
[c] Instrument Center, Faculty of Applied Sciences, University of Sri Jayewardenepura, Nugegoda 10250, Sri Lanka
[d] Department of Civil Engineering, University of Peradeniya, Peradeniya 20400, Sri Lanka
[e] The Institute of Agriculture, The University of Western Australia, Perth WA6009, Australia
[f] Sustainability Cluster, School of Engineering, University of Petroleum & Energy Studies, Dehradun, Uttarakhand 248007, India

ARTICLE INFO

ABSTRACT

Exposure to excess fluoride is a controversial public health concern as it can cause dental/skeletal fluorosis as well as renal toxicity. The study intended to evaluate the synergistic interaction of clay intercalation and thermochemical modification on corncob biochar to remove fluoride from aqueous solutions. Layered double hydroxide was assorted with thermally activated (torrefaction and pyrolysis) corncob biochar at 1:1 (w/w) ratio to obtain composites called LDH-CCBC250 and LDH-CCBC500. Physicochemically characterized adsorbents were assessed against the pH (3–9), reaction time (up to 12 h) and initial fluoride concentration (0.5–10 mg L^{-1}) for defluoridation. The porous structure of biochar was found to be richer compared to biocharcoal. The adsorption performance of LDH-CCBC500 was 6-fold higher compared to LDH-CCBC250 signifying the pronounced effect of thermal activation. Fluoride adsorption was pH dependent, and the best pH was in the range of pH 3.5–5.0 and there was no ionic strength dependency. Fluoride uptake by LDH-CCBC500 follows pseudo-second order and Elovich kinetic models, which suggests a chemisorption process followed by physisorption. The most expected way to eliminate fluoride by LDH-CCBC500, which had a maximum adsorption capacity of 7.24 mg g^{-1}, was cooperative chemical adsorption upon the Langmuir and Hills isotherm (r^2 = 0.99) parameters. Layered double hydroxide intercalated corncob biochar derived from slow pyrolysis is best performing in acidic waters.

1. Introduction

Fluoride (F$^-$) is a geogenic electronegative anionic contaminant found ubiquitously in groundwater sources. It was estimated that more than 200 million people expose to surplus F$^-$ concentrations (>1.5 mg L^{-1}) in drinking water in the world (Mohan et al., 2012; Vithanage and Bhattacharya, 2015). Groundwater contamination with excessive F$^-$ levels occurred naturally especially in semi-arid and arid regions of the world due to the chemical weathering of the rocks bearing fluoride-rich minerals (Yihunu et al., 2020; Hettithanthri et al., 2021). Long-term consumption of high F$^-$ concentrations which exceed the safe limits recommended by the World Health Organization (WHO) can cause serious health issues including skeletal and dental fluorosis. As a

Hofmeister ion chronic exposure to F$^-$ is considered to be a potential risk factor for the chronic kidney disease of unknown etiology (CKDu) in Sri Lanka (Hettithanthri et al., 2021). Hence, the need of effective technologies to reduce F$^-$ concentration in water/beverages to permissible levels is essential.

Adsorption has drawn more attention recently due to its simplicity and cost effectiveness. Among various adsorbents, biochar is considered as one of the most promising materials which produced by thermal treatments of biomass (Yaashikaa et al., 2020). These thermal processes can be either pyrolysis, pyrolytic gasification, hydro-thermal carbonization or torrefaction. The process conditions of the above methods such as heating rate, temperature and residence time are crucial in determining the physical and chemical properties of the product.

Pyrolysis is the most used traditional method for the production of biochar. In the slow pyrolysis, temperature ranges from 300 to 700 °C with a low heating rate of 5–7 °C min^{-1} and longer residence time for more than 1 h (Cantrell et al., 2012). High temperature (500–1000 °C), rapid heating rate around >100 °C min^{-1} and short residence time around 0.5–2 °C min^{-1} is known as fast pyrolysis (Mašek, 2016). The mild pyrogenic process under an oxygen-deficient environment at pyrolysis temperatures ranging from 200 to 300 °C is called torrefaction (Hu et al., 2020). In addition, torrefaction is the process through which biomass is converted into biocharcoal (Kwoczynski and Čmelík, 2021). It was evident that raising the pyrolysis temperature improves biochar's characteristics, particularly its specific surface areas and total pore volumes (Binh et al., 2022). Corncob is a cost-effective and locally available agro-based waste materials which is a byproduct of the corn (*Zea maize*) production process. Further, it is a promising and efficient green practice to convert large quantities of biomass waste into a useful value-added resource (Oni et al., 2019; Li et al., 2020). Interestingly, corncobs are fairly enriched in hemicellulose, cellulose, and lignin with a heterogeneous porous microstructure. Potato peel and rice husk biochar (2.91 mg g^{-1}), sawdust raw biochar (1.73 mg g^{-1}), and wheat straw raw biochar (1.93 mg g^{-1}) have exhibited relatively low F$^-$ adsorption performance (Yadav et al., 2013; Bibi et al., 2017; Kumar et al., 2020). However, modification processes are essential to enhance the adsorption capacity of pristine biochar (Vithanage et al., 2020). In order to increase the surface area and active functional groups of resultant biochar several modification strategies i.e. mineral modification, magnetic modification, carbonaceous nanomaterial modification, acid and alkaline activation are employed (Wang et al., 2020).

Tailoring biochar with clay minerals is one of the commonly used methods to improve physiochemical properties such as surface area, surface charges and surface active functional groups (Vithanage et al., 2020). Layered Double Hydroxides (LDHs), a synthetic hydrotalcite anionic clay have shown a great potential to remove F$^-$ from water with an excellent adsorption, specially in acidic water (Sun et al., 2017; Sarma and Rashid, 2018). LDHs have the basic chemical composition of $[M_{1-x}^{2+} M_x^{3+} (OH)_2]^{x+} (A^{n-})_{x/n}.yH_2O$ where M^{2+} represents a divalent cation, M^{3+} a trivalent cation, A^{n-} an interlayer anion with charge n, x is the di- and trivalent cations ratio, and y is the number of water moles. Indeed, it was reported that LDHs have an excellent exchangeable anionic capacity (3.0–4.8 meq g^{-1}) and outstanding thermal stability, which can make them a better option as an adsorbent specially for F$^-$ like negatively charged ions. The calcination process is responsible for the further increased anion exchange capacity of LDHs thus, adsorption capacity also increased over the corresponding uncalcined LDHs (Saba et al., 2019). However, due to the high adsorption in low pH environments and regeneration difficulties (due to dissolution), LDHs alone does not appear to be prospective (Sajid et al., 2022). Hence, engineered corncob biochar-LDH composite is a win-win and sustainable approach to the removal of contaminants in aqueous solutions (Alagha et al., 2020). Nonetheless, to the best of the authors' knowledge, synthesis and application of thermally activated (via torrefaction and pyrolysis) LDH modified corncob biocharcoal and biochar composites in the removal of F$^-$ in aqueous solution has not been reported. Therefore, the main objective of this study is to investigate the synergistic effects and F$^-$ adsorption efficiency of thermally (i.e. torrefaction and pyrolysis) and chemically (i.e. Mg/Fe LDH) modified corncob biocharcoal and biochar in aqueous solutions.

2. Materials and methodology

2.1. Material and chemicals

Analytical grade iron (III) chloride hexahydrate (FeCl$_3$·6H$_2$O) and magnesium chloride hexahydrate (MgCl$_2$·6H$_2$O) were purchased from Sigma Aldrich (Germany) and Daejung chemicals (Korea) respectively. Sodium chloride (NaCl) and sodium fluoride (NaF) were supplied by Sisco Research Laboratories (Pvt) Ltd (India). For pH adjustments, 0.1 M sodium hydroxide (NaOH) and nitric acid (HNO$_3$) were utilized. All experimental solutions were made with ultra-pure water (Smart2pure 6 UV, conductivity of 0.05 S cm^{-1}).

2.2. Biochar production

Corncob biomass was collected from a local farmland in a rural area, Sri Lanka. It was washed thoroughly with tap water, followed by distilled water to remove dust and any residues and air dried for 2 days. Then corncob were oven dried at 100 °C for 2 h. Dried biomass was sliced into small pieces prior to torrefaction and pyrolysis in the muffle furnace (Nabertherm, Germany). Finally, dried corncob pieces were torrefied at 250 °C and slow pyrolyzed at 500 °C for 2 h with a rate of 5 °C min^{-1} under a limited oxygen environment. In order to obtain fine particles, corncob biocharcoal (CCBC250) and biochar (CCBC500) were crushed with mortar and pestle.

2.3. LDH-biochar composite

Biochar-LDH composites were synthesized with co-precipitation technique using MgCl$_2$·6H$_2$O and FeCl$_3$·6H$_2$O salts as metal sources. An aqueous solution was prepared with Mg:Fe molar ratio of 1:3. The metal ion solution was added in dropwise at a rate of 5 mL min^{-1} into a beaker containing 1 M NaCl solution which contains 5 g of corncob biocharcoal (CCBC250) or biochar (CCBC500) with intensive stirring at room temperature (25 °C). The solution pH was controlled in the range of 9–10 throughout the process. The resulting precipitate was aged for 24 h at room temperature, centrifuged at 4000 rpm for 10 min and washed thoroughly with ultrapure water. The resulted precipitate was oven-dried at 60 °C for 24 h. Finally, the obtained precipitates were calcined at 150 °C for 2 h in a vacuum oven (VACIOTEM-T). Synthesized Mg/Fe-LDH augmented biocharcoal and biochar composites are referred as LDH-CCBC250 and LDH-CCBC500 respectively.

2.4. Materials characterization

Representative samples of biocharcoal and biochar composites were characterized for understand their physicochemical properties. The pH of the materials was determined with a 1:1 suspension of biochar/ultrapure water. Proximate analysis was conducted to assess the percentages of moisture, volatile matter, resident matter, and ash content of both biocharcoal and biochar samples (CCBC250 and CCBC500) (Ahmad et al., 2013). Field Emission Scanning Electron Microscopy (FE-SEM) at 15 kV was used to identify the surface morphology of the pristine biocharcoal/biochar and LDH-modified biochar/biocharcoal composites. Further, surface areas were determined by the Methylene Blue (MB) adsorption procedure (Tewari and Thornton, 2010). In brief, the adsorption of MB on adsorbents as a function concentration (0.5–12 mg L^{-1}) of adsorbate was observed by using 25 mg per 10 mL of dosage at room temperature. After 12 h of shaking time, the remaining MB concentration was measured spectrophotometrically at λ_{max} of 665 nm. The relationship between specific surface area and MB was determined using the given equation (1).

$$\text{Specific Surface Area (SSA)} = X_m \times N \times A \qquad (1)$$

where, X_m is the monolayers capacity (mol g^{-1}); N is Avagadro number (6.019 × 10^{23}) and A is area per molecule on the surface (130 Å^2).

Powder X-ray diffraction (PXRD) (Rigaku, Ultima IV, Japan) analysis was used to assess the mineralogical and crystalline structural parameters with a 20 min^{-1} scanning speed and a diffraction angle of 3–80 (2θ). The adsorbents were further characterized before and after the adsorption of F$^-$ ions using Fourier transform infrared spectroscopy (FTIR, ABB MB300) at room temperature. The zero-point charge (pH$_{PZC}$) of the adsorbents were determined by the surface titration with the Automatic

Potentiometric Titrator (HI931) (Campen et al., 2010).

2.5. Batch adsorption experiments

2.5.1. pH edge experiments

A series of batch experiments were conducted in triplicates to investigate the best adsorption conditions. Similar dosages of (1 g L^{-1}) CCBC250, CCBC500, LDH-CCBC250 and LDH-CCBC500 were separately added to 100 mL of 5 mg L^{-1} fluoride ion solution with three different ionic strengths (0.1, 0.01 and 0.001 M NaNO$_3$). The pH adjusted suspensions (pH = 3–10) were kept in a shaker (100 ppm) overnight at 25 °C to reach the equilibrium. Finally, samples were filtered using 0.45 μm syringe filters and F$^-$ concentrations were analyzed using Ion Chromatograph (IC) (Metrohm, 930 IC Flex).

2.5.2. Adsorption kinetic experiments

Sorption kinetics for composites was performed at the best ionic strength and pH which demonstrated the highest adsorption capacity. An initial F$^-$ concentration of 5 mg L^{-1} was spiked to an adsorbent dosage of 1 g L^{-1} in the presence of 0.01 M NaNO$_3$ ionic strength. At suitable time intervals (5–720 min) aliquots were withdrawn, filtered through a 0.45 μm syringe filter and then analyzed in the IC.

2.5.3. Adsorption isotherm experiments

The adsorption isotherm experiment to investigate the maximum F$^-$ adsorption capacity of LDH-CCBC250 and LDH-CCBC500 composites was conducted at pH of 4.0 and 0.01 M NaNO$_3$ ionic strength. A range of F$^-$ concentrations from 0.5 to 10 mg L^{-1} and adsorbent dosage of 1 g L^{-1} was used. Finally, samples were filtered and analyzed in IC.

2.6. Calculation and data modelling

The obtained data from kinetics and isotherm experiments were modelled using adsorption equations. Pseudo-first order, pseudo-second order and Elovich models were used in kinetic modelling whereas Langmuir, Freundlich isotherms and Hill models were applied in isotherm modelling.

The data modelling was performed using the OriginPro 2018 software package. The F$^-$ adsorption capacity and distribution coefficient (K_d) of the adsorbents were calculated using equations (2) and (3).

$$Q_e = \frac{(C_i - C_e)}{W} \tag{2}$$

$$Q_e = K_d \times C_e \tag{3}$$

Where, Q_e is the F$^-$ adsorption capacity (mg g^{-1}) at the equilibrium, C_i and C_e (mg L^{-1}) are initial and equilibrium F$^-$ concentrations respectively, and W (g L^{-1}) is the adsorbent dosage.

3. Results and discussions

3.1. Materials characterization

3.1.1. Physicochemical characteristics of CCBC types and composites

Physicochemical characteristics of biocharcoal, biochar and composites are listed in Table 1. A decrease in biochar yield was observed from 48.3 to 19.7% with increased pyrolysis temperature. This elaborates the demolition of polysaccharides such as cellulose and hemicellulose. Lignin is very resistant to thermal degradation and it starts to decompose and release as pyrolytic vapour beyond 500 °C. Further, organic materials are subjected to combust at high temperatures resulting a decline in yield. Moreover, the ash % of biochar was elevated from 5.64% to 9.25%, while volatile matter content was reduced from 85.95% to 56.0% with increasing temperatures from 250 to 500 °C. Similarly, the rate at which volatile components are converted into low

Table 1
The physiochemical characteristics of each biochar and composite.

	CCBC250	CCBC500	LDH-CCBC250	LDH-CCBC500
(a) Proximate analysis				
pH	5.34	9.55	10.12	10.28
Moisture %	7.52	5.62	-	-
Volatile matter %	85.95	56.00	-	-
Ash %	5.64	9.25	-	-
Resident matter %	0.90	29.13	-	-
Yield %	48.3	19.7	82	83
(b) Point of zero charge (pH$_{PZC}$)	-	-	9.6	9.0

molecular weight liquids and gases increases as the pyrolysis temperature rises (Ronsse et al., 2013).

Nevertheless, increased temperature promotes the formation of inorganic elements in biochar which results in high ash % (Keiluweit et al., 2010; Rafiq et al., 2016). The pH of biocharcoal (CCBC250) was acidic (pH = 5) whereas biochar (CCBC500) was alkaline. High pH may responsible for the separation of alkali salts from the organics matrix (Yuan et al., 2011).

The pHpzc of LDH-CCBC250 and LDH-CCBC500 composites were 9.6 and 9.0, respectively. Therefore, both composite surfaces were positively charged at the experimental solutions. Chemical and electrostatic characteristics of surface functional groups govern pH$_{PZC}$ and play an important role in elucidating adsorption mechanisms. However, the composite surface area was determined by the adsorption of methylene blue onto LDH-CCBC500 (83 m^2 g^{-1}) and LDH-CCBC250 (744 m^2 g^{-1}) (Tewari and Thornton, 2010). The large difference between the adsorption capacities may be caused by the influence of pore structures and functional groups on the adsorbent surface resulted by the temperature variation (Hao et al., 2013). Further, pores on CCBC500 could be blocked by LDH during the modification which results low methylene blue adsorption interpreting low specific surface area.

3.1.2. Surface morphology analysis

Biochar surfaces appear to be porous as depicted by the images (Fig. 1A and B). Due to the pyrolyzed temperature variation, there is a notable difference in the porous structure. Results showed that the CCBC250 had a lot of microporous structures less than 10 μm uniformly arranged as a web. Nevertheless, the surface of CCBC500 clearly reveals irregular and cave-type channels. Related literature reveals well-defined channel arrays in biochar pyrolyzed at low temperatures whereas different pore diameters for biochar pyrolyzed at high temperatures (Rafiq et al., 2016; Binh et al., 2022). A large number of mesopores ranging from 10 to 20 μm were observed on the CCBC500 surface, which can positively influence the modification process. The emergence of mesopores in the CCBC500 might be caused to mobile matter escaping from the feedstock during the pyrolysis at high temperatures (Ahmad et al., 2012). After LDH modification the pores of CCBC500 were unevenly filed with LDH, which happened to increase the surface area accessible to interact with adsorbate molecules.

3.1.3. Surface chemistry analyses

Few notable chemical changes have occurred in composites as corncob biomass is heated to 250 and 500 °C (Fig. 2). The hydrogen-bonded hydroxyl groups (O–H) are represented by the peaks at 3331, 3436, and 3420 cm^{-1} (Atugoda et al., 2021). The peak broadening of the LDH-CCBC250 and LDH-CCBC500 composites spectra compared to the pristine CCBC250 and CCBC500 might be due to the introduction of LDH in the chemical activation. In CCBC250, a peak was observed at 1632 cm^{-1}, which signifies the presence of aromatic C=C or C=O of either ketones or quinones (Uchimiya et al., 2011). However, the mentioned peak has shifted in CCBC500 (1589 cm^{-1}) indicating the influence of increasing temperature from 250 to 500 °C. The peak which lies at 1379
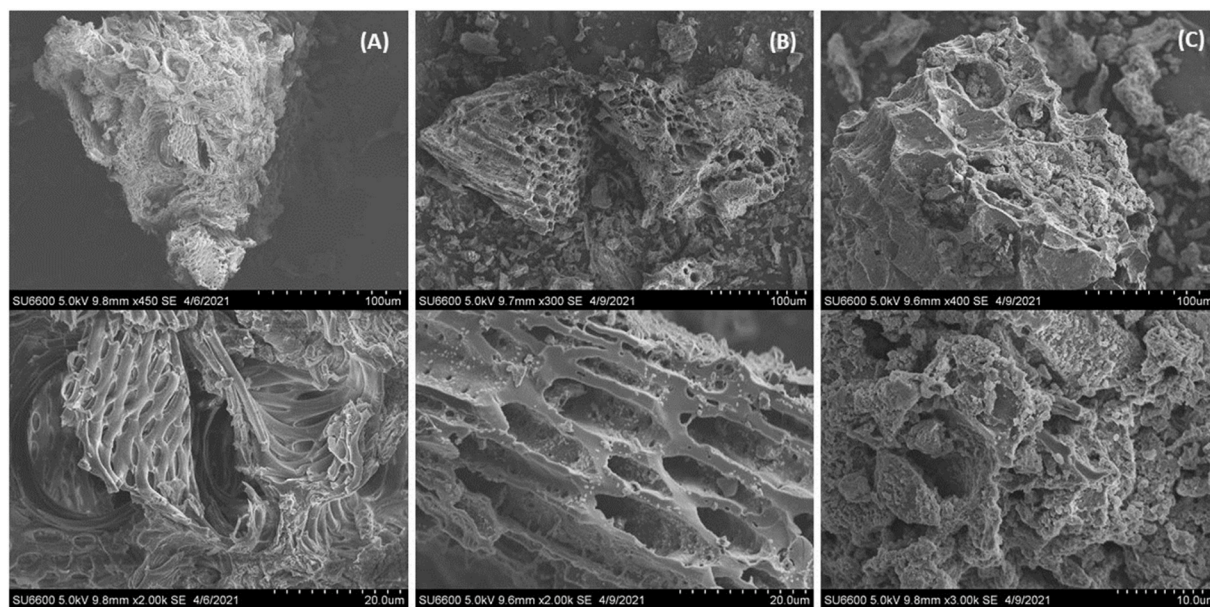
Fig. 1. The SEM images of CCBC250 at magnification × 450 and × 2.00 k (A), CCBC500 at magnification × 300 and × 2.00 k (B), and LDH-CCBC500 at magnification × 400 and × 3.00 k (C).
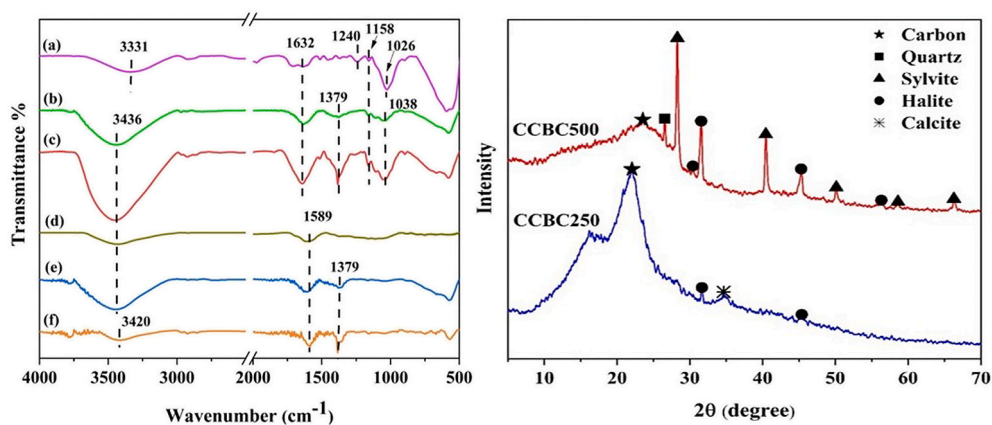
Fig. 2. Left: FTIR spectrums for (a) CCBC250, (b) LDH-CCBC250, (c) fluoride treated LDH-CCBC250, (d) CCBC500, (e) LDH-CCBC500, (f) fluoride treated LDH-CCBC500 in aqueous media (pH 4.0), Right: PXRD pattern of CCBC250 and CCBC500 biochars.

cm^{-1}, was mainly attributable to the bending of phenolic –OH or C–O (Keiluweit et al., 2010). The peak at 1379 cm^{-1} was visible only in LDH-CCBC250 and LDH-CCBC500 composites suggesting the incorporation of LDH in the modification. Nevertheless, the intensity of bending of phenolic –OH or C–O was remarkably increased in F^- treated spectra corroborating the incorporation of F^- with both composites. The C–O–C stretching vibrations of phenolic groups associated with lignin were observed at 1240 cm^{-1} (Tomczyk et al., 2020). The band observed at 1158 cm^{-1} which is the stretching vibration of C–O, demonstrates the characteristics of cellulose-like structures. Symmetric C–O stretching at 1026 cm^{-1} in pristine CCBC250 has shifted to 1038 cm^{-1} in LDH-CCBC250 composite regardless of F^- adsorption (Correia et al., 2017). In addition, some peaks (i.e. 1038, 1026, 1158, 1240 cm^{-1}) of LDH-CCBC250 (Fig. 2a-c) which lie in the range of 750–1250 cm^{-1} were diminished in the LDH-CCBC500 (Fig. 2d-f). However, compared to biochar and its modified composite, biocharcoal and its modified composite showed more functional groups than that of the biochar and its composite obviously due to high temperature. This proves thermochemical modification of biochar influences the surface functional groups (Yadav and Jagadevan, 2021).

The generation of a heterogeneous surface was identified by XRD

patterns of CCBC250 and CCBC500, which confirms that raising the pyrolysis temperature has resulted higher number of narrow, sharp peaks in the biochar compared to biocharcoal (Fig. 2). The broad diffraction peak at 2θ = 16–23° in CCBC250 can be attributed to amorphous carbon structures (Siddique et al., 2018; Astuti et al., 2020). Further, few low-intensity peaks at 2θ = 31.5 and 45.4° have observed in the XRD spectrum of CCBC250 which indicates the presence of sodium chloride (NaCl) and calcite ($CaCO_3$) at 2θ = 34.6° (Zornoza et al., 2016). Apart from the aforementioned peaks, the presence of any crystalline phases was not observed in the XRD spectrum of CCBC250. It is important to note that the elevated number of peaks in CCBC500 XRD spectrum indicates the presence of many inorganic elements for instant sylvite, halite and calcite, which is further proven by high ash content in proximate analysis. Contrary, the increasing temperature has led to the disappearance of characteristic cellulose crystallinity in CCBC500. Peaks at 2θ = 30.5, 31.5, 45.4 and 56.5° correspond to the presence of NaCl mineral. Further, reflections at 2θ = 28.2, 40.4, 50.1, 58.6, and 66.4° have revealed the presence of sylvite (KCl) in XRD pattern of CCBC500 (Pipíška et al., 2022). However, the peak at 2θ = 26.6° indicates the availability of quartz (SiO_2) in CCBC500. The X-ray diffractograms confirmed that biochar possesses a heterogeneous surface with many

mineral elements over biocharcoal.

3.2. Effect of pH on fluoride elimination

The amount of F^- adsorbed by CCBC250, CCBC500 and LDH-CCBC250 was comparatively low in the experimental pH range (Fig. 3). When the solution pH is from 3.5 to 5, the adsorption capacity of LDH-CCBC500 has reached its highest value between 2 and 2.5 mg g^{-1}. However, the adsorption of F^- by LDH-CCBC500 composite has not considerably influenced by increasing NaNO$_3$ concentration (Fig. 4). The continued increase of pH (more than 5.5) has led to a notable decline in the adsorption capacity of all four adsorbents. However, LDH modification could not influence much on the adsorption capacity of the LDH-CCBC250 composite. Therefore, LDH-CCBC500 composite is more suitable for the defluoridation of water at any ionic strength. The K$_d$ values for the LDH-CCBC500 were higher than LDH-CCBC250 at pH range 3–7, indicating its high capacity for F^- adsorption. According to the pH$_{PZC}$ both composites were favourable for the adsorption of F^-. However, there is an obvious influence of functional groups on F^- binding capacity to the surface over pH$_{PZC}$.

3.3. Adsorption kinetics

The influence of contact time for F^- adsorption on LDH modified corncob biochar composites (pyrolyzed at 250 and 500 °C) up to 12 h is shown in Fig. 5. At first, the rate of F^- adsorption on both LDH-CCBC250 and LDH-CCBC500 composites was rapid, then slowed down with increasing reaction time. Both LDH-CCBC250 and LDH-CCBC500 composites have reached the equilibrium state after 250 min. The availability of vacant active sites increases the adsorption of F^- and gradually decreases with time due to the saturation of binding sites (Atugoda et al., 2021). Therefore, isotherm experiment was carried out for 250 min as no substantial removal of F^- was observed afterwards. Interestingly, the overall adsorption capacity of LDH-CCBC500 composite is higher than LDH-CCBC250.

In order to understand the adsorption kinetic mechanism for LDH-modified corncob biochar composites, the obtained data have been modelled using pseudo-first order, pseudo-second order, and Elovich models (Table 2). Compared to Elovich kinetic model pseudo-second order model (maximum $r^2 = 0.95$ and least $\chi^2 = 0.006$) perfectly fitted well with LDH-CCBC250 experimental data. Therefore, F^- ions have adsorbed to LDH-CCBC250 via chemical bond formation which is chemisorption process. However, obtained data for F^- ions adsorption to LDH-CCBC250 also gives a better fit with Elovich model ($r^2 = 0.94$ and $\chi^2 = 0.007$) confirming the contribution of chemical forces to the adsorption of F^- ions on heterogeneous surface of LDH-CCBC250. Furthermore, the adsorption data for LDH-CCBC500 was modelled

with the 3 kinetic models similar to LDH-CCBC250. Pseudo-second order model was the best fitted model with a maximum correlation coefficient (r^2) value of 0.98 and the least χ^2 of 0.017. Nevertheless, both pseudo-first order and Elovich models were also fitted for the adsorption kinetic data with a similar correlation coefficient of 0.96. Thus, F^- adsorption process of LDH-CCBC500 is governed by chemisorption followed by physisorption. The initial F^- adsorption rate (α) of LDH-CCBC500 was enhanced compared to LDH-CCBC250 indicating favorability of F^- adsorption by LDH-CCBC500 composite.

3.4. Adsorption isotherm

The adsorption isotherm data for LDH-CCBC250 and LDH-CCBC500 was modelled with Langmuir, Freundlich and Hills non-linear curve fits. A two-step process was observed in the LDH-CCBC250 (Fig. 6a). The first phase of the adsorption gave an excellent fit to the Langmuir isotherm model ($r^2 = 0.98$) with the maximum monolayer adsorption capacity (q_{max}) of 1.15 mg g^{-1}. Further, Langmuir constant (K_L) is greater than 0 and less than 1 suggesting favourable adsorption. This describes the surface of LDH-CCBC250 composite is saturated with monolayer adsorption of F^- ions in lower concentrations. Nevertheless, energetically equivalent adsorption is suggested by the Langmuir model. It was observed that the first phase of LDH-CCBC250 isotherm data were perfectly fitted with Langmuir model whereas second phase fairly fitted both Freundlich and Hills isotherms models. This indicates the involvement of chemisorption during low concentrations and physisorption at high concentrations. However, a better fit was obtained with the Hills model ($r^2 = 0.99$) compared to the Freundlich model ($r^2 = 0.97$) denoting that the binding of different species was taking place on a homogeneous substrate of LDH-CCBC250. Nevertheless, publication of multi-step isotherm curves in the field of water decontamination is rather limited.

The absorption of F^- by LDH-CCBC500 composite has been reduced with the increased F^- concentration due to the homogenous binding sites. The experimental data for LDH-CCBC500 was modelled with the Langmuir, Freundlich and Hills isotherms models (Fig. 6b). Based on high r^2 (0.99) and low χ^2 (0.009) values, both Langmuir and Hills isotherm models were perfectly fitted. Thus, it is evident that monolayer adsorption of F^- has taken place on the surface consisting of limited active sites following chemisorption. Positive cooperative adsorption can be predicted since the Hill cooperativity coefficient (b) is greater than 1 for both LDH-CCBC250 and LDH-CCBC500. This assumes that the binding of F^- on one active site could influence the other binding sites on the same adsorbent (Atugoda et al., 2021). The maximum adsorption capacity of LDH-CCBC500 composite is six times more (7.24 mg g^{-1}) than the LDH-CCBC250 composite, confirming that pyrolysis can considerably enhance the F^- adsorption.
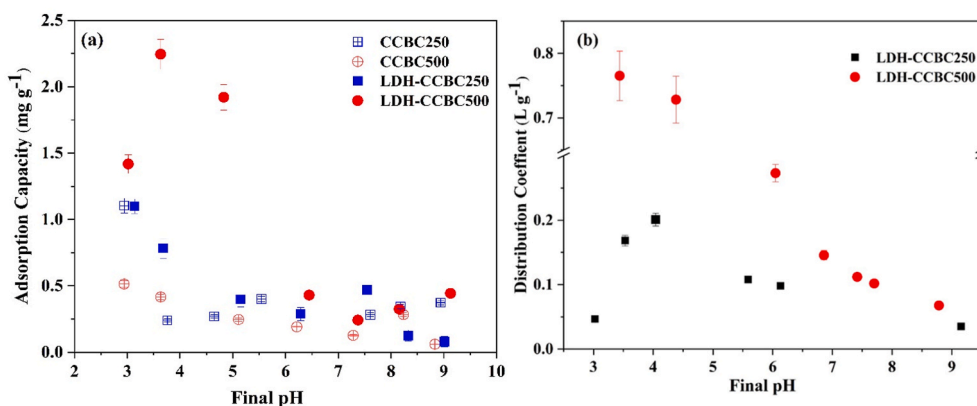
Fig. 3. Influence of pH on fluoride adsorption by (a) CCBC250, CCBC500, LDH-CCBC250, LDH-CCBC500 and (b) variation of distribution coefficients (K$_d$) in the pH range of 3–9 for fluoride-loaded LDH-CCBC250 and LDH-CCBC500, dosage 1 g L^{-1}, initial fluoride concentration 5 mg L^{-1} at 25 °C.
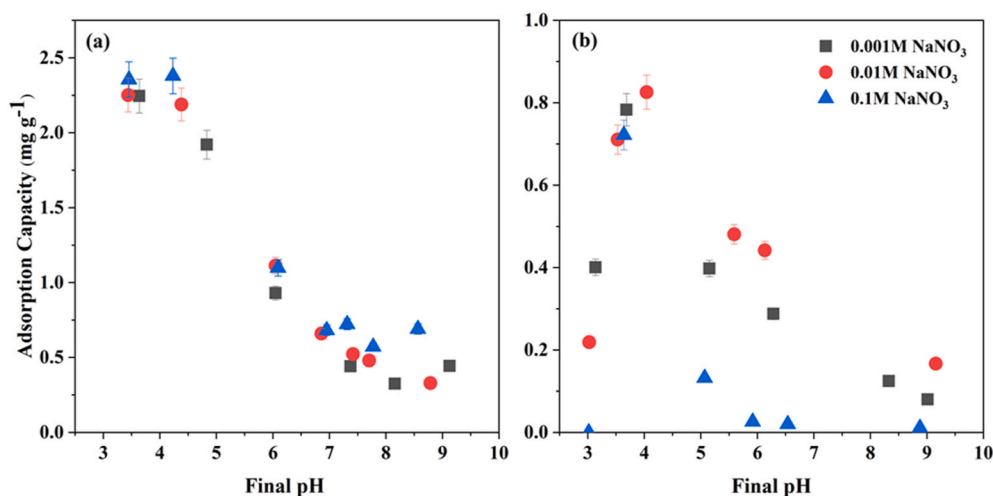
Fig. 4. The adsorption of fluoride on (a) LDH-CCBC250 and (b) LDH-CCBC500 at different ionic strengths, dosage = 1 g L^{-1}, C$_0$ = 5 mg L^{-1}, and at 25 °C. Standard deviation of the average is shown by error bars (n = 3).
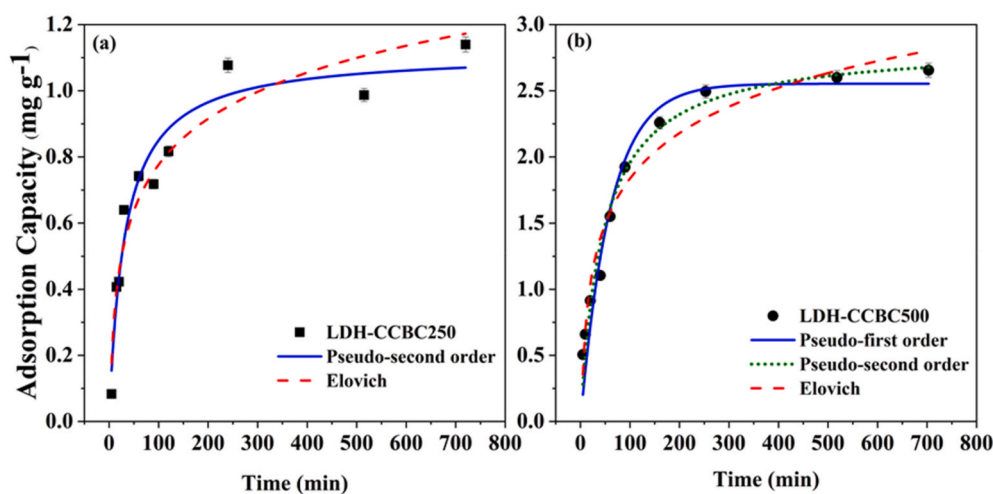
Fig. 5. Influence of time on fluoride elimination by (a) LDH-CCBC250 and (b) LDH-CCBC500 at 1 g L^{-1} adsorbent dosage and pH 4 with 5 mg L^{-1} fluoride concentration in 0.01 M NaNO$_3$ of background ionic strength.

3.5. Postulated sorption mechanism

The adsorption mechanisms can be well explained and understood by the modelled kinetic and isotherm data. High adsorption rate and short equilibrium time predict the relatively high density of active sites on the adsorbents surfaces. At pH < pH$_{PZC}$, protonation of the hydroxide groups (–OH^{2+}) on the adsorbent surface encourage the formation of positively charged active sites. Therefore, negatively charged F$^-$ ions form hydrogen bonds via electrostatic attractions resulting in enhanced defluoridation. Presence of strong H-bonds have identified in F$^-$ adsorbed LDH-CCBC500 displacement and the low intensity of –OH stretching vibration (3436–3420 cm^{-1}).

Moreover, the positively charged Mg^{2+} and Fe^{3+} in the composite showed an attractive tendency toward F$^-$ ions involves in the F$^-$ adsorption via electrostatic attraction (Eq. 4-5; Me denoted as cationic ions and R denoted as carbon chain). However, with the increased solution pH, the positively charged binding sites on the composites reduced and became more negatively charged heading to deprotonation.

Despite of adsorption, F$^-$ ions can replace interlayer anion of the composite (Cl$^-$ ions) via ion exchange mechanism, which is another postulation for F$^-$ removal. Moreover, ion exchange can take place between adsorbate and adsorbent since the bonding affinity towards F$^-$ is greater than hydroxyl ions. The shifting and intensity reduction of the –OH peaks before and after adsorption are clear indications of these interactions (Fig. 2).

Additionally, protonated groups facilitate the ligand exchange mechanism between F$^-$ and composites surface via strong forces (Eq. 6-7). Fluoride has lone pair electrons which can donate to the divalent or trivalent metal ions by forming metal-fluoride complexes. Moreover, it is possible that pore filling also contributes to the F$^-$ absorption mechanism owing to the porous nature of the material (Fig. 1C). Interestingly, all of these interactions are supported by the composites' surface heterogeneity.

$$R–Me–OH_2^+ + F^- \rightarrow R–Me–OH_2 \cdots F \quad (4)$$

$$MeOH_2^+ + F^- \rightarrow MeOH_2 \cdots F \quad (5)$$

$$MeOH + F^- \rightarrow MeF + OH^- \quad (6)$$

$$Me(OH)_2^- + 2 F^- \rightarrow MeF_2 + 2OH^- \quad (7)$$
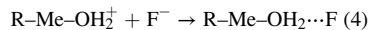
Table 2

Model parameters for the LDH-CCBC250 and LDH-CCBC500 for the kinetic and isothermal adsorption of fluoride at pH 4.

Kinetic model fitting

Model	Equation	Description	Parameter	LDH-CCBC250	LDH-CCBC500
Pseudo-first order	$q_t = q_e(1 - e^{(k_1 \times t)})$	q_e: equilibrium adsorption capacity k_1: rate constant	k_1 (min^{-1}) q_e (mg g^{-1}) r^2 χ^2	–	0.02 ± 0.002 2.55 ± 0.09 0.96 0.031
Pseudo-second order	$q_t = \dfrac{(k_2 \times t \times q_e^2)}{(1 + k_2\, q_e\, t)}$	q_e: equilibrium adsorption capacity k_2: rate constant	k_2 (g mg^{-1} min^{-1}) q_e (mg g^{-1}) r^2 χ^2	0.03 ± 0.01 1.12 ± 0.05 0.95 0.006	0.01 ± 0.001 2.85 ± 0.10 0.98 0.017
Elovich	$q_t = \dfrac{1}{\beta} ln(\alpha\beta) + \dfrac{1}{\beta} ln(t)$	α: initial F$^-$ adsorption rate β: desorption constant related to the amount of surface coverage	α (mg g^{-1} min^{-1}) β (g mg^{-1}) r^2 χ^2	0.09 ± 0.02 4.98 ± 0.44 0.94 0.007	0.20 ± 0.04 2.02 ± 0.14 0.96 0.029

Isotherm model fitting

Model	Equation	Description	Parameter	LDH-CCBC250	LDH-CCBC500
Langmuir	$q_e = \dfrac{(q_{max} K_L C_e)}{(1 + K_L C_e)}$	K_L: Langmuir constant q_{max}: maximum adsorption capacity	K_L (L mg^{-1}) q_{max} (mg g^{-1}) r^2 χ^2	0.16 ± 0.11 1.15 ± 0.61 0.98 0.0002	0.09 ± 0.02 7.24 ± 1.06 0.99 0.009
Freundlich	$q_e = K_f C_e^n$	K_f: Freundlich constant related to the adsorption capacity n: adsorption intensity	K_f (mg g^{-1})/(mg L^{-1})$^{-n}$ n r^2 χ^2	0.094 ± 0.02 1.14 ± 0.13 0.97 0.006	0.63 ± 0.05 0.77 ± 0.05 0.98 0.018
Hills	$q_e = \dfrac{q_{max}\,(K_h C_e)^b}{1 + (K_h C_e)^b}$	K_h: Hill constant b: Hill cooperativity coefficient q_{max}: maximum adsorption capacity	K_h b q_{max} (mg g^{-1}) r^2 χ^2	0.15 ± 0.06 2.12 ± 0.67 1.69 ± 0.59 0.99 0.004	0.17 ± 0.07 1.19 ± 0.16 5.01 ± 1.19 0.99 0.009

Fig. 6. Isotherm modelling of the adsorption of fluoride onto the (a) LDH-CCBC250 and (b) LDH-CCBC500 composites at pH 4 (contact time 12 h and adsorbent dose 1 g L^{-1} at 25 °C). (Standard deviation of the average is shown by error bars (n = 3)).

3.6. Comparison of modified biochar adsorbents

The ability of biochar treated with different chemicals to remove F$^-$ from aqueous solutions is continually being studied. A comparison of the distribution coefficients (K$_d$) along with optimum conditions of selected adsorbents towards F$^-$ was summarized in Table 3. Limited number of studies have been carried out to investigate the simultaneous impact of the thermochemical modification on F$^-$ adsorption. Nevertheless, LDH-modified corncob biochar is an efficient and cost-effective material to remove F$^-$ with a low adsorbent dose at room temperature. Some adsorbents such as aluminum impregnated coconut fiber ash, La–Fe–Al modified rice husk biochar, and Zirconium dioxide modified *Camellia oleifera* seed shell exhibit high K$_d$ values however, the chemicals used in the modification process are not cost-effective. Synthesized composite

can be successfully applied in home-scale water purification systems in areas where groundwater is acidic in nature. Less adsorption capacity in normal environmental pH is identified as a major drawback of the study for its commercial applications.

4. Conclusion

This study has been conducted to investigate the F$^-$ removal capacity using LDH modified corncob biochar (LDH-CCBC500) and corncob biocharcoal (LDH-CCBC250). It has been found out that LDH-CCBC500 composite is successful in removing F$^-$ from aqueous medium. Low pH values (ex.pH 4) have increased the adsorption while alkaline pHs reduced the selectivity of the active sites for F$^-$ sorption. Therefore, LDH-CCBC500 is an effective adsorbent for F$^-$ in acidic water or

Table 3
Characteristics of several biochar-modified adsorbents with regard to fluoride adsorption.

Biochar modified adsorbent	Optimum pH	Temperature (°C)	Zero point pH	BET surface area (m² g⁻¹)	Dosage (g L⁻¹)	Equilibrium time (min)	Initial concentration (mg L⁻¹)	Adsorption capacity (mg g⁻¹)	Distribution coefficient/K_d (L g⁻¹)	References
Zirconium modified cashew nut shell	7	30	4.2	–	0.015	180	2–10	1.83	0.195	Alagumuthu and Rajan (2010)
Aluminum impregnated coconut fiber ash	5	40	7.2	26.3	0.05	60	1–10	1.13	1.130	Mondal et al. (2015)
Aluminum modified pine sawdust	6	25	8.34	–	0.5	120	5–100	2.89	0.003	Vázquez-Guerrero et al. (2016)
Lanthanum-modified pomelo peel biochar	6.5	25	5.8	269.48	1	1440	10–300	5.03	0.503	Wang et al. (2018)
Zirconium dioxide modified *Camellia oleifera* seed shell	6.8	45	4.45	–	1.6	180	5–70	11.04	0.636	Mei et al. (2020)
Iron modified rice husk biochar (700 °C)	4	30	6	196.11	4	120	5–35	4.45	0.253	Yadav and Jagadevan (2021)
La–Fe–Al (1:1:3) modified rice husk biochar (500 °C)	7	25	–	95.36	1	30	6–160	111.11	0.983	Zhou et al. (2022)
Layered double hydroxide modified corncob biocharcoal (250 °C)	**4**	**25**	**9.6**	**744** [a]	**1**	**250**	**0.5–10**	**1.69**	**0.224**	**This study**
Layered double hydroxide modified corncob biochar (500 °C)	**4**	**25**	**9.0**	**83**[a]	**1**	**250**	**0.5–10**	**7.24**	**0.570**	

[a] Methylene blue method.

beverages since F^- in low pH solutions is detrimental to health. Furthermore, ionic strength had no obvious impact on the adsorption capacity of LDH-CCBC500 and it allows effective F^- removal in high ion concentration environments. In addition, maximum defluoridation capacity is recorded as 7.24 mg g⁻¹ at 25 °C by LDH-CCBC500. Despite the fact that biocharcoal has more functional groups than biochar, results confirm that LDH-CCBC500 has a greater capacity for adsorption of F^- through pore filling than LDH-CCBC250 does. Further, the electrostatic attractions, ion exchange interactions, and ligand exchange mechanisms clearly describe how F^- is removed from an aqueous solution by the LDH-CCBC500 composite. This study suggests that LDH assorted corncob biochar composite can be used as a promising adsorbent for F^- removal in acidic aqueous media. Nonetheless, future research studies should concentrate on synthesis of a feasible adsorbent for the adsorptive removal of F^- from groundwater in the presence of counterions. Besides, further modifications are essential to enhance the F^- adsorption in groundwater at neutral pH values.

Author statement

Declaration of competing interest

Data availability

Data will be made available on request.

Acknowledgements

References

Ahmad, M., Lee, S.S., Dou, X., Mohan, D., Sung, J.-K., Yang, J.E., Ok, Y.S., 2012. Effects of pyrolysis temperature on soybean stover- and peanut shell-derived biochar properties and TCE adsorption in water. Bioresour. Technol. 118, 536–544. https://doi.org/10.1016/j.biortech.2012.05.042.

Ahmad, M., Lee, S.S., Rajapaksha, A.U., Vithanage, M., Zhang, M., Cho, J.S., Lee, S.-E., Ok, Y.S., 2013. Trichloroethylene adsorption by pine needle biochars produced at various pyrolysis temperatures. Bioresour. Technol. 143, 615–622. https://doi.org/10.1016/j.biortech.2013.06.033.

Alagha, O., Manzar, M.S., Zubair, M., Anil, I., Mu'azu, N.D., Qureshi, A., 2020. Comparative adsorptive removal of phosphate and nitrate from wastewater using biochar-MgAl LDH nanocomposites: coexisting anions effect and mechanistic studies. Nanomaterials 10 (2), 336. https://doi.org/10.3390/nano10020336.

Alagumuthu, G., Rajan, M., 2010. Equilibrium and kinetics of adsorption of fluoride onto zirconium impregnated cashew nut shell carbon. Chem. Eng. J. 158 (3), 451–457. https://doi.org/10.1016/j.cej.2010.01.017.

Astuti, F., Sari, N., Maghfirohtuzzoimah, V.L., Asih, R., Baqiya, M.A., Darminto, D., 2020. Study of the formation of amorphous carbon and rGO-like phases from palmyra sugar by variation of calcination temperature. Jurnal Fisika dan Aplikasinya 16 (2), 91–94.

Atugoda, T., Gunawardane, C., Ahmad, M., Vithanage, M., 2021. Mechanistic interaction of ciprofloxacin on zeolite modified seaweed (Sargassum crassifolium) derived biochar: kinetics, isotherm and thermodynamics. Chemosphere 281, 130676. https://doi.org/10.1016/j.chemosphere.2021.130676.

Bibi, S., Farooqi, A., Yasmin, A., Kamran, M.A., Niazi, N.K., 2017. Arsenic and fluoride removal by potato peel and rice husk (PPRH) ash in aqueous environments. Int. J. Phytoremediation 19 (11), 1029–1036. https://doi.org/10.1080/15226514.2017.1319329.

Binh, Q.A., Nguyen, V.-H., Kajitvichyanukul, P., 2022. Influence of pyrolysis conditions of modified corn cob bio-waste sorbents on adsorption mechanism of atrazine in contaminated water. Environ. Technol. Innovat. 26, 102381 https://doi.org/10.1016/j.eti.2022.102381.

Campen, R.K., Pymer, A.K., Nihonyanagi, S., Borguet, E., 2010. Linking surface potential and deprotonation in nanoporous silica: second harmonic generation and acid/base titration. J. Phys. Chem. C 114 (43), 18465–18473. https://doi.org/10.1021/jp1037574.

Cantrell, K.B., Hunt, P.G., Uchimiya, M., Novak, J.M., Ro, K.S., 2012. Impact of pyrolysis temperature and manure source on physicochemical characteristics of biochar. Bioresour. Technol. 107, 419–428.

Correia, R., Gonçalves, M., Nobre, C., Mendes, B., 2017. Impact of torrefaction and low-temperature carbonization on the properties of biomass wastes from Arundo donax L. and Phoenix canariensis. Bioresour. Technol. 223, 210–218. https://doi.org/10.1016/j.biortech.2016.10.046.

Hao, F., Zhao, X., Ouyang, W., Lin, C., Chen, S., Shan, Y., Lai, X., 2013. Molecular structure of corncob-derived biochars and the mechanism of atrazine sorption. Agron. J. 105 (3), 773–782.

Hettithanthri, O., Sandanayake, S., Magana-Arachchi, D., Wanigatunge, R., Rajapaksha, A.U., Zeng, X., Shi, Q., Guo, H., Vithanage, M., 2021. Risk Factors for Endemic Chronic Kidney Disease of Unknown Etiology in Sri Lanka: Retrospect of Water Security in the Dry Zone. Science of The Total Environment, p. 795. https://doi.org/10.1016/j.scitotenv.2021.148839, 148839.

Hu, H., Lv, C., Hu, A., Wang, T., Lu, H., 2020. Influence of torrefaction intensities on bamboo (Acidosasa longiligula) shoot shell-derived biochar and its application for Tc (VII) reductive immobilization. J. Taiwan Inst. Chem. Eng. 116, 266–271. https://doi.org/10.1016/j.jtice.2020.11.011.

Keiluweit, M., Nico, P.S., Johnson, M.G., Kleber, M., 2010. Dynamic molecular structure of plant biomass-derived black carbon (biochar). Environ. Sci. Technol. 44 (4), 1247–1253. https://doi.org/10.1021/es9031419.

Kumar, P., Prajapati, A.K., Dixit, S., Yadav, V.L., 2020. Adsorption of fluoride from aqueous solution using biochar prepared from waste peanut hull. Mater. Res. Express 6 (12), 125553. https://doi.org/10.1088/2053-1591/ab6ca0.

Kwoczynski, Z., Čmelík, J., 2021. Characterization of biomass wastes and its possibility of agriculture utilization due to biochar production by torrefaction process. J. Clean. Prod. 280, 124302 https://doi.org/10.1016/j.jclepro.2020.124302.

Li, S., Chan, C.Y., Sharbatmaleki, M., Trejo, H., Delagah, S., 2020. Engineered biochar production and its potential benefits in a closed-loop water-reuse agriculture system. Water 12 (10), 2847. https://doi.org/10.3390/w12102847.

Mašek, O., 2016. 21 - biochar in thermal and thermochemical biorefineries—production of biochar as a coproduct. In: LUQUE, R., LIN, C.S.K., WILSON, K., CLARK, J. (Eds.), Handbook of Biofuels Production, second ed. Woodhead Publishing.

Mei, L., Qiao, H., Ke, F., Peng, C., Hou, R., Wan, X., Cai, H., 2020. One-step synthesis of zirconium dioxide-biochar derived from Camellia oleifera seed shell with enhanced removal capacity for fluoride from water. Appl. Surf. Sci. 509, 144685 https://doi.org/10.1016/j.apsusc.2019.144685.

Mohan, D., Sharma, R., Singh, V.K., Steele, P., Pittman Jr., C.U., 2012. Fluoride removal from water using bio-char, a green waste, low-cost adsorbent: equilibrium uptake and sorption dynamics modeling. Ind. Eng. Chem. Res. 51 (2), 900–914. https://doi.org/10.1021/ie202189v.

Mondal, N.K., Bhaumik, R., Datta, J.K., 2015. Removal of fluoride by aluminum impregnated coconut fiber from synthetic fluoride solution and natural water. Alex. Eng. J. 54 (4), 1273–1284. https://doi.org/10.1016/j.aej.2015.08.006.

Oni, B.A., Oziegbe, O., Olawole, O.O., 2019. Significance of biochar application to the environment and economy. Ann. Agric. Sci. (Cairo) 64 (2), 222–236. https://doi.org/10.1016/j.aoas.2019.12.006.

Pipíška, M., Krajčíková, E.K., Hvostik, M., Frišták, V., Ďuriška, L., Černičková, I., Kaňuchová, M., Conte, P., Soja, G., 2022. Biochar from wood chips and corn cobs for adsorption of thioflavin T and erythrosine B. Materials 15 (4). https://doi.org/10.3390/ma15041492.

Rafiq, M.K., Bachmann, R.T., Rafiq, M.T., Shang, Z., Joseph, S., Long, R., 2016. Influence of pyrolysis temperature on physico-chemical properties of corn stover (Zea mays L.) biochar and feasibility for carbon capture and energy balance. PLoS One 11 (6), e0156894.

Ronsse, F., Van Hecke, S., Dickinson, D., Prins, W., 2013. Production and characterization of slow pyrolysis biochar: influence of feedstock type and pyrolysis conditions. Gcb Bioenergy 5 (2), 104–115. https://doi.org/10.1111/gcbb.12018.

Saba, J., Afaaf, R.A., Shanza, R.K., Muhammad, R.S.A.J., 2019. Layered double hydroxides (LDHs): synthesis & applications. Prog. Chem. 31 (2/3), 394–412. https://doi.org/10.7536/PC180505.

Sajid, M., Sajid Jillani, S.M., Baig, N., Alhooshani, K., 2022. Layered double hydroxide-modified membranes for water treatment: recent advances and prospects. Chemosphere 287, 132140. https://doi.org/10.1016/j.chemosphere.2021.132140.

Sarma, G.K., Rashid, M.H., 2018. Synthesis of Mg/Al layered double hydroxides for adsorptive removal of fluoride from water: a mechanistic and kinetic study. J. Chem. Eng. Data 63 (8), 2957–2965. https://doi.org/10.1021/acs.jced.8b00242.

Siddique, A.B., Pramanick, A.K., Chatterjee, S., Ray, M., 2018. Amorphous carbon dots and their remarkable ability to detect 2,4,6-trinitrophenol. Sci. Rep. 8 (1), 9770. https://doi.org/10.1038/s41598-018-28021-9.

Sun, Z., Park, J.-S., Kim, D., Shin, C.-H., Zhang, W., Wang, R., Rao, P., 2017. Synthesis and adsorption properties of Ca-Al layered double hydroxides for the removal of aqueous fluoride. Water, Air, Soil Pollut. 228 (1), 1–7. https://doi.org/10.1007/s11270-016-3240-0.

Tewari, B.B., Thornton, C.O., 2010. Use of basic Methylene Blue Dye for specific surface area measurement of metal hexacyanoferrate (II) complexes. Rev. Soc. Quim. Peru 76 (4), 330–335.

Tomczyk, A., Sokołowska, Z., Boguta, P., 2020. Biochar physicochemical properties: pyrolysis temperature and feedstock kind effects. Rev. Environ. Sci. Biotechnol. 19 (1), 191–215.

Uchimiya, M., Wartelle, L.H., Klasson, K.T., Fortier, C.A., Lima, I.M., 2011. Influence of pyrolysis temperature on biochar property and function as a heavy metal sorbent in soil. J. Agric. Food Chem. 59 (6), 2501–2510. https://doi.org/10.1021/jf104206c.

Vázquez-Guerrero, A., Alfaro-Cuevas-Villanueva, R., Rutiaga-Quiñones, J.G., Cortés-Martínez, R., 2016. Fluoride removal by aluminum-modified pine sawdust: effect of competitive ions. Ecol. Eng. 94, 365–379. https://doi.org/10.1016/j.ecoleng.2016.05.070.

Vithanage, M., Ashiq, A., Ramanayaka, S., Bhatnagar, A., 2020. Implications of Layered Double Hydroxides Assembled Biochar Composite in Adsorptive Removal of Contaminants: Current Status and Future Perspectives. Science of The Total Environment, p. 737. https://doi.org/10.1016/j.scitotenv.2020.139718, 139718.

Vithanage, M., Bhattacharya, P., 2015. Fluoride in the environment: sources, distribution and defluoridation. Environ. Chem. Lett. 13 (2), 131–147. https://doi.org/10.1007/s10311-015-0496-4.

Wang, J., Chen, N., Feng, C., Li, M., 2018. Performance and mechanism of fluoride adsorption from groundwater by lanthanum-modified pomelo peel biochar. Environ. Sci. Pollut. Control Ser. 25 (16), 15326–15335. https://doi.org/10.1007/s11356-018-1727-6.

Wang, L., Ok, Y.S., Tsang, D.C.W., Alessi, D.S., Rinklebe, J., Wang, H., Mašek, O., Hou, R., O'Connor, D., Hou, D., 2020. New trends in biochar pyrolysis and modification strategies: feedstock, pyrolysis conditions, sustainability concerns and implications for soil amendment. Soil Use Manag. 36 (3), 358–386.

Yaashikaa, P.R., Kumar, P.S., Varjani, S., Saravanan, A., 2020. A critical review on the biochar production techniques, characterization, stability and applications for circular bioeconomy. Biotechnology Reports 28, e00570. https://doi.org/10.1016/j.btre.2020.e00570.

Yadav, A.K., Abbassi, R., Gupta, A., Dadashzadeh, M., 2013. Removal of fluoride from aqueous solution and groundwater by wheat straw, sawdust and activated bagasse carbon of sugarcane. Ecol. Eng. 52, 211–218. https://doi.org/10.1016/j.ecoleng.2012.12.069.

Yadav, K., Jagadevan, S., 2021. Influence of torrefaction and pyrolysis on engineered biochar and its applicability in defluoridation: insight into adsorption mechanism, batch adsorber design and artificial neural network modelling. J. Anal. Appl. Pyrol. 154, 105015 https://doi.org/10.1016/j.jaap.2021.105015.

Yihunu, E.W., Yu, H., Junhe, W., Kai, Z., Teffera, Z.L., Weldegebrial, B., Limin, M., 2020. A comparative study on defluoridation capabilities of biosorbents: isotherm, kinetics, thermodynamics, cost estimation and regeneration study. Environmental Engineering Research 25 (3), 384–392. https://doi.org/10.4491/eer.2019.097.

Yuan, J.-H., Xu, R.-K., Zhang, H., 2011. The forms of alkalis in the biochar produced from crop residues at different temperatures. Bioresour. Technol. 102 (3), 3488–3497. https://doi.org/10.1016/j.biortech.2010.11.018.

Zhou, N., Guo, X., Ye, C., Yan, L., Gu, W., Wu, X., Zhou, Q., Yang, Y., Wang, X., Cheng, Q., 2022. Enhanced fluoride removal from drinking water in wide pH range using La/Fe/Al oxides loaded rice straw biochar. Water Supply 22 (1), 779–794. https://doi.org/10.2166/ws.2021.232.

Zornoza, R., Moreno-Barriga, F., Acosta, J.A., Muñoz, M.A., Faz, A., 2016. Stability, nutrient availability and hydrophobicity of biochars derived from manure, crop residues, and municipal solid waste for their use as soil amendments. Chemosphere 144, 122–130. https://doi.org/10.1016/j.chemosphere.2015.08.046.